Draft version June 13, 2025
Typeset using LaTeX **twocolumn** style in AASTeX7

Dust Budget Crisis in Little Red Dots

Kejian Chen [1,2] Zhengrong Li [1,2] Kohei Inayoshi [1] and Luis C. Ho [1,2]

[1] *Kavli Institute for Astronomy and Astrophysics, Peking University, Beijing 100871, China*
[2] *Department of Astronomy, School of Physics, Peking University, Beijing 100871, China*

ABSTRACT

Little red dots (LRDs), a population of active galactic nuclei (AGNs) recently identified by JWST, are characterized by their compact morphology and red optical continuum emission, which is often interpreted as evidence for significant dust extinction of $A_V \gtrsim 3$ mag. However, the dust-reddened AGN scenario is increasingly challenged by their faint near-to-far infrared emission and a potential "dust budget crisis" in cases when the host galaxy is either undetectably low-mass or absent. In this study, we re-evaluate the dust extinction level in LRDs by modeling the UV-to-infrared spectra for various extinction laws and a broad range of dusty distribution parameters. Comparing the predicted infrared fluxes with observational data from the JWST MIRI, Herschel, and ALMA, our analysis finds that the visual extinction is tightly constrained to $A_V \lesssim 1.0$ mag for A2744-45924 and $A_V \lesssim 1.5$ mag for RUBIES-BLAGN-1 under the SMC extinction laws, with slightly weaker constraints for those with gray extinction in the UV range. The revised A_V values yield a radiative efficiencies of 10% for the LRD population, easing the tension with the Sołtan argument for the bulk AGN population at lower redshifts. Moreover, this moderate extinction (or dust-free) scenario, with reprocessed emission spectra testable by future far-infrared observatories, provides a paradigm shift in understanding their natures, environments, and evolutionary pathways of massive black holes in the early universe.

Keywords: Galaxy formation (595) — High-redshift galaxies (734) — Quasars (1319) — Supermassive black holes (1663) — Interstellar medium (847)

1. INTRODUCTION

The James Webb Space Telescope (JWST) has uncovered a new type of active galactic nuclei (AGNs), known as little red dots (LRDs), characterized by broad emission lines, red continuum spectra, and compact morphology (D. D. Kocevski et al. 2023; J. Matthee et al. 2024; J. E. Greene et al. 2024; V. Kokorev et al. 2023; B. Wang et al. 2024a; I. Labbe et al. 2025a). This new population is $\sim 1-2$ orders of magnitude more abundant than luminous quasars, reaching $\gtrsim 1\%$ of the abundance of star-forming galaxies at redshifts of $z \sim 4-7$ (D. D. Kocevski et al. 2024; V. Kokorev et al. 2024; H. B. Akins et al. 2024), and is considered to represent a key building block and crucial growth phase of seed black holes (BHs) that power quasars at later epochs (S. Fujimoto et al. 2022). Moreover, the population emerges at high redshifts and rapidly disappears toward lower redshifts (D. D. Kocevski et al. 2024; Y. Ma et al. 2025a; Euclid Collaboration et al. 2025), possibly transitioning into more typical AGN populations by losing the LRD characteristics (K. Inayoshi 2025).

A well-defined feature of broad-line AGNs observed as LRDs is their characteristic v-shaped spectral energy distribution (SED), composed of red optical and blue UV continua emission with a turnover wavelength near the Balmer limit (D. D. Kocevski et al. 2023; G. Barro et al. 2024; J. Matthee et al. 2024; J. E. Greene et al. 2024; K. N. Hainline et al. 2025; D. J. Setton et al. 2024). Although the origin of this distinctive SED has been poorly understood, the red component is often interpreted as dust-reddened systems with extinction levels of $A_V \sim 3$ mag, suggesting scenarios involving dusty star-forming galaxies, AGNs, or some combination of both (B. Wang et al. 2024a). However, JWST MIRI observations have revealed that the rest-frame near-infrared (NIR) fluxes of LRDs tend to be fainter than expected from hot dust heated by UV/optical radiation sources (P. G. Pérez-González et al. 2024; H. B. Akins et al. 2024; G. C. K. Leung et al. 2024; D. J. Setton et al. 2025). To satisfy these MIRI flux constraints (or upper limit if non-detection is reported), dust distri-

Email: chenkejian@stu.pku.edu.cn, lizhengrong@pku.edu.cn

bution should be either spatially extended (Z. Li et al. 2025), unlike the compact dusty tori commonly found in AGNs, or highly clumpy (M. Nenkova et al. 2008; S. F. Hönig & M. Kishimoto 2010, and its application to the LRD context in C. M. Casey et al. 2024). Both the scenarios effectively shift the dust emission peak from the NIR ($\simeq 1-5\ \mu$m) to the mid-infrared (MIR; $\simeq 5-35\ \mu$m) bands. Furthermore, non-detection of LRDs in ALMA suggests that dust is as warm as $\sim$ 100 K, substantially higher than that led by active star formation (I. Labbe et al. 2025b; H. B. Akins et al. 2024; M. Xiao et al. 2025). C. M. Casey et al. (2025) also reported non-detection of stacking deep ALMA observations for 60 LRDs, providing a stringent upper limit on the dust mass below $10^6\ M_\odot$.

Additionally, there is no clear observational evidence for host galaxies associated with LRDs. This might not be surprising as LRDs are typically selected as point-like sources in imaging from longer-wavelength channels of JWST NIRCam. In some cases, extended UV components have been detected (M. Killi et al. 2024; C.-H. Chen et al. 2025b,a; P. Rinaldi et al. 2024), but these features are often spatially offset from the central LRD or show surface brightness profiles with low central concentration. For the underlying host galaxies, if present, stringent upper limits on the stellar mass are placed at $\log(M_\star/M_\odot) < 8.3-9.6$ based on imaging decomposition and spectral fitting (C.-H. Chen et al. 2025b). If the LRD population indeed lacks stellar hosts, or contains only minimal stellar component, this raises a critical question: *where do the metals and dust grains responsible for reddening the AGN originate?* The possible absence of host galaxies highlights a potential "dust budget crisis" for LRDs.

In this *Letter*, we revisit the dust-reddening hypothesis for LRD spectra and assess its necessity. Assuming that the observed UV-to-optical spectra of LRDs result from dust-reddening with a given extinction level A_V, we reconstruct the expected IR emission from dust heated by the central radiation source. By comparing the predicted reprocessed IR SED with current observations, we find that the upper limits on A_V for two broad-line LRDs with rest-frame UV-to-IR coverage (B. Wang et al. 2024b; I. Labbe et al. 2024; D. J. Setton et al. 2025) are constrained as low as $A_V \lesssim 0.5-1.5$ mag, depending on the assumed dust reddening law. This moderate level of dust extinction challenges the conventional interpretations of LRDs as heavily obscured AGNs, and instead motivates a paradigm shift in understanding their properties, environments, and potential connection to their descendant populations.

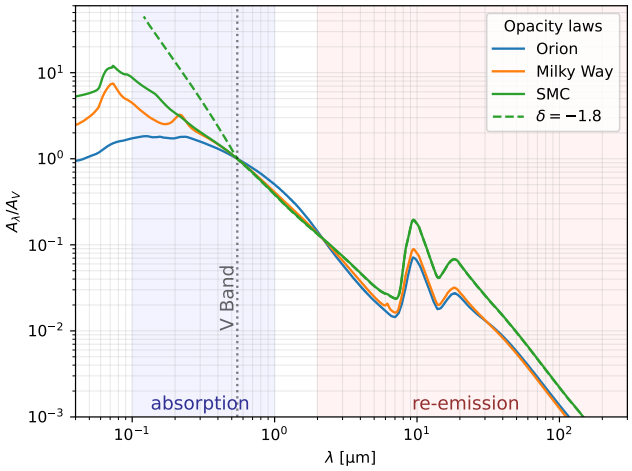

Figure 1. Extinction curves as a function of wavelength used in this work, covering from UV to infrared wavelengths: the SMC, the interstellar dust in the Milky Way with $R_V = 3.1$ (J. C. Weingartner & B. T. Draine 2001), and the Orion Nebula (J. A. Baldwin et al. 1991). We also show the modified Calzetti's attenuation law proposed in S. Noll et al. (2009) with $\delta = -1.8$ (see main text). The extinction A_λ is normalized at the V band 5500 Å (dotted vertical line). The UV to optical part is used to compute dust attenuation of the incident radiation flux (blue shaded region), and the IR part is used to calculate the re-emission from heated dust (red shaded region).

2. METHOD

2.1. *Dust opacity*

In this work, we adopt three different dust extinction laws: the Small Magellanic Cloud (SMC), the Milky Way (MW) interstellar medium (MW) dust (J. C. Weingartner & B. T. Draine 2001) with $R_V = 3.1$, and the Orion Nebula dust (J. A. Baldwin et al. 1991). Figure 1 shows the wavelength dependence of the dust opacity for each model. In our analysis, the UV to optical parts of the extinction curves are used to compute the attenuation of the incident radiation flux (blue shaded region), while the IR parts are used to estimate the re-emission from heated dust (red shaded region). Among the three models, the SMC extinction curve shows a steep wavelength dependence at $0.1 \lesssim \lambda/\mu\text{m} \lesssim 0.5$, whereas the Orion Nebula extinction curve remains relatively flat at $\lambda \lesssim 0.3\ \mu$m. The MW extinction law shows the bump feature of 2175 Å possibly from small carbonaceous grains and/or polycyclic aromatic hydrocarbon (PAH) molecules, which is absent in the other cases likely due to destruction by irradiation from central hot sources and size growth in dense environments (e.g. W. T. Reach et al. 2000). At longer wavelengths, all models converge to a single power-law behavior following the electric dipole approximation $A_\lambda \propto \lambda^{-2}$ (B. T.

Draine 2011), with two prominent bumps of silicate features at 9.7 μm and 18 μm (e.g., L. Hao et al. 2007).

In addition to the extinction curves described above, we consider a flexible dust attenuation law originally proposed in S. Noll et al. (2009) as

$$A_\lambda = A_V \cdot \frac{k'(\lambda)}{R'_V} \left(\frac{\lambda}{0.55\ \mu\mathrm{m}} \right)^\delta, \quad (1)$$

where $R'_V = 4.05$ and $k'(\lambda)$ is the polynomial function provided by Equation (4) in D. Calzetti et al. (2000). The power-law index δ controls the slope of the attenuation curve in the UV band: the curve becomes steeper than the original Calzetti law when $\delta < 0$. Although S. Noll et al. (2009) initially introduced the index δ to provide moderate flexibility ($-0.3 < \delta < 0.3$) for fitting normal star-forming galaxies, this functional form has also been used to explain the spectral shape of some LRDs, which shows stronger UV attenuation than the SMC law (corresponding to $\delta \simeq -0.5$) (e.g. B. Wang et al. 2024b; Y. Ma et al. 2025b; I. Labbe et al. 2024; A. de Graaff et al. 2025). For instance, the SEDs of A2744-45924 and RUBIES-BLAGN-1 are fitted with $\delta = -1.79$ (I. Labbe et al. 2024) and $\delta = -1.21$ (B. Wang et al. 2024b), respectively. Motivated by these results, we test a case with a steep attenuation law of $\delta = -1.8$ at $0.12 \leq \lambda/\mu\mathrm{m} \leq 0.55$ and revert to the SMC law at longer wavelengths (dashed curve in Figure 1)[3].

To compute the absolute level of extinction and re-emission of radiation, we normalize the dust opacity using the relative extinction curve, A_λ/A_V, by defining the extinction and absorption cross sections at photon frequency $\nu(= c/\lambda)$ per hydrogen atom; $\sigma_\nu^{\rm ext}$ and $\sigma_\nu^{\rm abs}$, respectively. The extinction cross section is expressed as $\sigma_\nu^{\rm ext} = \sigma_V^{\rm ext}(A_\lambda/A_V)$. In this work, we adopt a reference value of $\sigma_V^{\rm ext} = 3.72 \times 10^{-23}$ cm^2 $(Z/0.1\ Z_\odot)(\mathcal{D}_\odot/0.01)$, where $\mathcal{D}_\odot = 0.01$ is the dust-to-gas mass ratio at solar metallicity. We assume the dust-to-gas ratio scales linearly with metallicity as $\mathcal{D} = \mathcal{D}_\odot(Z/Z_\odot)$.

Although $\sigma_\nu^{\rm abs}$ generally differs from $\sigma_\nu^{\rm ext}$ due to the contribution of scattering in the latter, the scattering properties are not well constrained from observations. Therefore, for simplicity, we assume $\sigma_\nu^{\rm abs} = \sigma_\nu^{\rm ext}$ throughout this study.

2.2. *Dust re-emission*

In this section, we describe our method for computing the reprocessed IR spectrum $L_\nu^{\rm re\text{-}emit}$, given an incident AGN spectrum $L_\nu^{\rm inc}$, a dust density distribution following the gas number density profile $n(r)$, and dust cross section per hydrogen atom σ_ν (R. Barvainis 1987). Our approach builds upon the method presented in Z. Li et al. (2025) by implementing various dust opacity laws and exploring a wider range of physical parameters.

We assume a power-law radial density profile, $n(r) = n_0(r/r_{\rm in})^{-\gamma}$, defined between the inner and outer radii, $r_{\rm in}$ and $r_{\rm out}$, where n_0 is the density at the inner edge and the power-law index varies in a range of $0 \leq \gamma \leq 2$. The inner edge ($r_{\rm in}$) is determined by the dust sublimation condition, where the dust temperature equals a threshold of $T_{\rm sub} = 1500$ K. The sublimation temperature generally depends on the grain composition and the ambient gas density, ranging $T_{\rm sub} \simeq 1000 - 2000$ K for $10 < n_0/{\rm cm}^{-3} < 10^{10}$ (A. Baskin & A. Laor 2018): graphite grains have a threshold temperature higher by ~ 300 K than that of silicate grains. Within the uncertainty, the upper limit of A_V changes only by $\simeq 0.1$ mag. Given these physical parameters, the outer radius ($r_{\rm out}$) is set by the required column density $N_{\rm H}(r_{\rm out})$, where $N_{\rm H}(r) = \int_{r_{\rm in}}^{r} n(r')dr'$, by solving the closure relation of $A_V = 1.086\ \sigma_V^{\rm ext} N_{\rm H}(r_{\rm out})$.

With this dust distribution, the dust temperature profile $T_{\rm dust}(r)$ is obtained by balancing radiative heating from the incident AGN light and cooling through dust thermal emission as

$$\int \frac{L_\nu^{\rm inc}}{4\pi r^2} e^{-\tau_\nu(r)} \sigma_\nu^{\rm abs} {\rm d}\nu = 4\pi \int B_\nu[T_{\rm dust}(r)]\ \sigma_\nu^{\rm abs} {\rm d}\nu, \quad (2)$$

where the optical depth is $\tau_\nu(r) = \sigma_\nu^{\rm ext} N_{\rm H}(r)$, $B_\nu(T)$ is the Planck function with a dust temperature $T = T_{\rm dust}$, and the spectrum is integrated over the entire spectral range. Using the temperature profile, $T_{\rm dust}(r)$, the re-emitted IR spectrum is calculated as

$$L_\nu^{\rm re\text{-}emit} = \Omega \int_{r_{\rm in}}^{r_{\rm out}} \sigma_\nu^{\rm abs} B_\nu[T_{\rm dust}(r)]\ n(r) 4\pi r^2 {\rm d}r, \quad (3)$$

where the solid angle Ω covered by the dusty medium is taken to be 4π.

Based on the density profile and A_V value, the total dust mass is estimated as

$$M_{\rm dust} = \mathcal{D} m_p \int_{r_{\rm in}}^{r_{\rm out}} n(r) 4\pi r^2 {\rm d}r, \quad (4)$$

with a dust-to-gas mass ratio $\mathcal{D}$ for metallicity $Z = 0.1 Z_\odot$.

2.3. *An upper limit on A_V*

In the previous section, we described the forward modeling approach, which begins with the incident SED and then computes the IR re-emission flux for a given set of

[3] The shorter-wavelength part of the attenuation model with $\delta = -1.8$ is not considered because the polynomial fitting function $k'(\lambda)$ of the Calzetti law is given only at $\lambda \geq 0.12$ μm. As discussed in Section 2.3, omitting the incident radiation flux at $\lambda < 0.12$ μm leads to a conservative upper limit on A_V.

dust properties. However, the incident SED is not observable, and the nature of LRDs is still debated, from pure galaxies (e.g. B. Wang et al. 2024a) to pure AGN (e.g. D. D. Kocevski et al. 2023; Z. Li et al. 2025), even some peculiar models (e.g. R. P. Naidu et al. 2025; A. de Graaff et al. 2025). In this study, we thus assume that the observed SED of LRDs results from dust reddening and infer the incident SED by assigning a specific value of visual extinction A_V as

$$L_\nu^{\rm inc} = L_\nu^{\rm obs}\, 10^{0.4(A_\lambda/A_V)A_V}, \quad (5)$$

where A_λ/A_V is given by the dust opacity laws (see Figure 1). We here consider two representative LRDs with spectroscopic redshifts and broad emission lines detected by JWST NIRSpec, along with photometric coverage from rest-frame UV/optical (NIRCam) and NIR (MIRI). The first is A2744-45924, the brightest LRD discovered to date, at $z_{\rm spec} = 4.4655$ (I. Labbe et al. 2024). The second is RUBIES-BLAGN-1, a luminous LRD at $z_{\rm spec} = 3.1034$ (B. Wang et al. 2024b). Figure 2 presents photometric flux densities for A2744-45924, which exhibits clear AGN signatures (broad Hα emission seen in the NIRCam grism; I. Labbe et al. 2024), but show no evidence of strong NIR or FIR dust emission; neither is detected by MIRI or ALMA, suggesting the lack of both hot and cold dust components (D. J. Setton et al. 2025). RUBIES-BLAGN-1 also shows similar spectral features in JWST and ALMA (D. J. Setton et al. 2025), with UV luminosity ~ 5 times lower than A2744-45924. Moreover, the two objects have no obvious host galaxy signatures and are consistent with point-source morphology. In the case of A2744-45924, two extended emission components are visible, but they are spatially offset from the AGN and are consistent with foreground galaxies, with SED fitting yielding a photometric redshift of $z_{\rm photo} \simeq 1.02$ (C.-H. Chen et al. 2025a).

The primary criterion for deriving an upper limit on A_V is that the predicted IR re-emission flux, $L_\nu^{\rm re\text{-}emit}(A_V)$, calculated as described in Section 2.2, must not exceed the observed flux or the upper limits from non-detections in any photometric band. To quantify this, we define the function

$$f(A_V) = \max_{\nu\in\{\nu_i\}} \left[\log_{10} L_\nu^{\rm re\text{-}emit}(A_V) - \log_{10} L_\nu^{\rm obs}\right], \quad (6)$$

where $\{\nu_i\}$ denotes the set of photon frequencies corresponding to the pivot wavelength of photometric filters. The upper limit of A_V is defined by solving $f(A_V) = 0$. We note that this constraint yields a conservative estimate of the maximum allowed A_V value, since the observed IR flux should also include a contribution from the the dust-extinguished part of the intrinsic emission, in addition to the reprocessed component. This method also allows us to identify which observational data provide a more stringent constraint on the A_V upper limit.

It is worth noting that we do not include extreme ultraviolet (EUV) emission at rest-frame $\lambda \lesssim 0.1{-}0.12\ \mu$m in the incident SED due to the lack of spectral data. Although AGNs are known to be powerful ionizing radiation sources as observed in the spectra of low-redshift AGNs unaffected by intergalactic medium absorption, the intrinsic EUV properties of LRDs remain highly uncertain. If the EUV contribution were included in our analysis, it would further heat the surrounding dusty medium and enhance the resulting reprocessed IR flux. Therefore, omitting the EUV component leads to a conservative upper limit on A_V.

3. RESULTS

In this section, we describe the predicted SED spanning rest-frame UV to IR wavelengths, computed for several combinations of A_V, γ and n_0. We also provide upper limits of A_V where the resulting SEDs remain consistent with *all* available observational data for the two LRDs (A2744-45924 and RUBIES-BLAGN-1), though we focus on the result for A2744-45924 in Sections 3.1 and 3.2 because the two cases yield similar conclusions (see Section 3.3).

3.1. *Multi-wavelength SEDs of LRDs*

We first consider the observed SED of the brightest LRD (A2744-45924; I. Labbe et al. 2024). In the left panel of Figure 2, we present both the incident SED and the corresponding IR re-emission spectra for our fiducial model, which adopts $(\gamma, n_0) = (0.5, 10^3\ {\rm cm}^{-3})$ and the SMC opacity law. As the value of A_V increases from 0.2 to 1.0 mag, the incident (de-reddened) SED inferred from the observed SED using Equation (5) becomes brighter significantly at shorter wavelengths due to the steep UV rise in the SMC extinction curve (see Figure 1). The corresponding energy absorbed by dust is reprocessed and re-emitted in the IR band, shown by solid curves. For $A_V \leq 0.4$ mag, the re-emitted IR flux remains below the observed flux data. However, for $A_V \sim 0.6$ mag, the predicted IR flux approaches or exceeds the MIRI F2100W detection, thereby violating the observational constraint. Using the method described in Section 2.3, we determined the maximum allowed extinction for this dust distribution to be $A_V = 0.55$ mag.

In the right panel of Figure 2, we compare four representative models with different values of (γ, n_0). For each case, its re-emission IR spectrum is given with the upper limit of A_V. We present the same model as in the left panel where $(\gamma, n_0) = (0.5, 10^3\ {\rm cm}^{-3})$, but with the

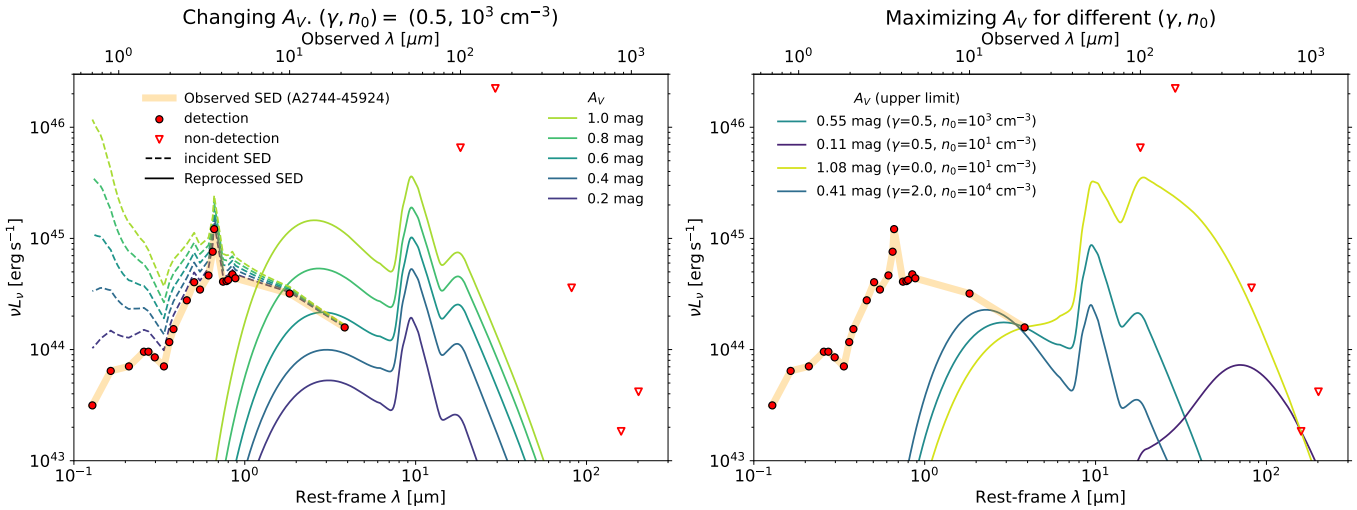

Figure 2. Multi-wavelength SED of the brightest LRD, A2744-45924 (orange curve) with JWST NIRCam/MIRI detection (circles) and non-detection in Herschel and ALMA bands (triangles). *Left*: Incident (corrected for extinction) and reprocessed IR re-emission spectra for fixed dust distribution parameters $\gamma = 0.5$ and $n_0 = 10^3$ cm^{-3} with varying visual extinction A_V. *Right*: Re-emission SEDs for four different dust density configurations: $(\gamma, n_0) = (0.5, 10^3\ \mathrm{cm}^{-3})$, $(0.5, 10\ \mathrm{cm}^{-3})$, $(0, 10\ \mathrm{cm}^{-3})$, and $(2.0, 10^4\ \mathrm{cm}^{-3})$. For each case, the maximum allowed A_V is applied such that the resulting IR flux does not violate the observational constraints.

upper limit of $A_V = 0.55$ mag. This parameter combination leads to a high average dust temperature of $T_{\rm dust} \gtrsim 200$ K, resulting in strong emission in the NIR. The second model with $(\gamma, n_0) = (0.5, 10\ \mathrm{cm}^{-3})$ has a more extended and diffuse dust distribution. This leads to significant FIR re-emission from the outer region, tightly constrained by ALMA non-detection. Thus, a stricter upper limit of $A_V \simeq 0.11$ mag is given in this case. The third model with $(\gamma, n_0) = (0, 10\ \mathrm{cm}^{-3})$ shifts most energy into the MIR band. Since the Herschel constraints in this band are relatively shallow, the corresponding A_V upper limit is more relaxed to 1.08 mag. Yet, this value remains substantially lower than ~ 3 mag typically assumed in previous studies (D. J. Setton et al. 2025). The fourth model assumes a dense and concentrated density profile with $(\gamma, n_0) = (2.0, 10^4\ \mathrm{cm}^{-3})$. This model is motivated by the physical connection to dense nuclear scales (see Section 4.3). While this SED shows rest-frame NIR bump, the flux density remains consistent with JWST MIRI data (F1000W and F2100W) due to moderate extinction of $A_V \simeq 0.41$ mag.

3.2. *Parameter surveys*

Here, we systematically investigate how the upper limit on A_V depends on the dust distribution, n_0 and γ, considering both the SMC and Orion Nebula extinction laws. The observational constraints are taken from JWST/MIRI, Herschel/PACS, and ALMA data for A2744-45924 (I. Labbe et al. 2024; D. J. Setton et al. 2025). Figure 3 summarizes the distribution maximum allowed A_V for each combination of (n_0, γ). The star symbols correspond to the parameter sets for the four models shown in the right panel of Figure 2. We overlay curves (white dashed) indicating constant dust masses estimated with the density distribution parameters (γ, n_0) and the associated A_V upper limit.

The left panel of Figure 3 shows the A_V upper limits derived using the SMC extinction law. The allowed values of A_V vary significantly across the parameter space. In the upper-left region, characterized by high n_0 and low γ, the A_V constraint is primarily given by MIRI observations and becomes tighter, as these models produce strong NIR/MIR emission from warm dust $T_{\rm dust} \gtrsim 200$ K and exceed the observed fluxes unless A_V is sufficiently low. In contrast, in the lower-right region, low n_0 and high γ, the constraint is dominated by ALMA non-detections, since these models yield significant FIR emission from colder dust ($T_{\rm dust} \gtrsim 30$ K). The black solid line marks the boundary separating the MIRI- and ALMA-constrained regimes. The right-hand side of the red curve (i.e., steeper profiles with lower n_0) indicates the region where the dust distribution is far extended to $r_{\rm out} \geq 10$ kpc to achieve sufficient column density. We rule out the domain as unphysical configurations. For the SMC opacity model, the least restrictive constraint appears at $(\gamma, n_0) \approx (0, 10\ \mathrm{cm}^{-3})$, where the upper limit reaches $A_V \simeq 1$ mag.

The right panel of Figure 3 presents the results assuming the Orion Nebula extinction law. A key differ-

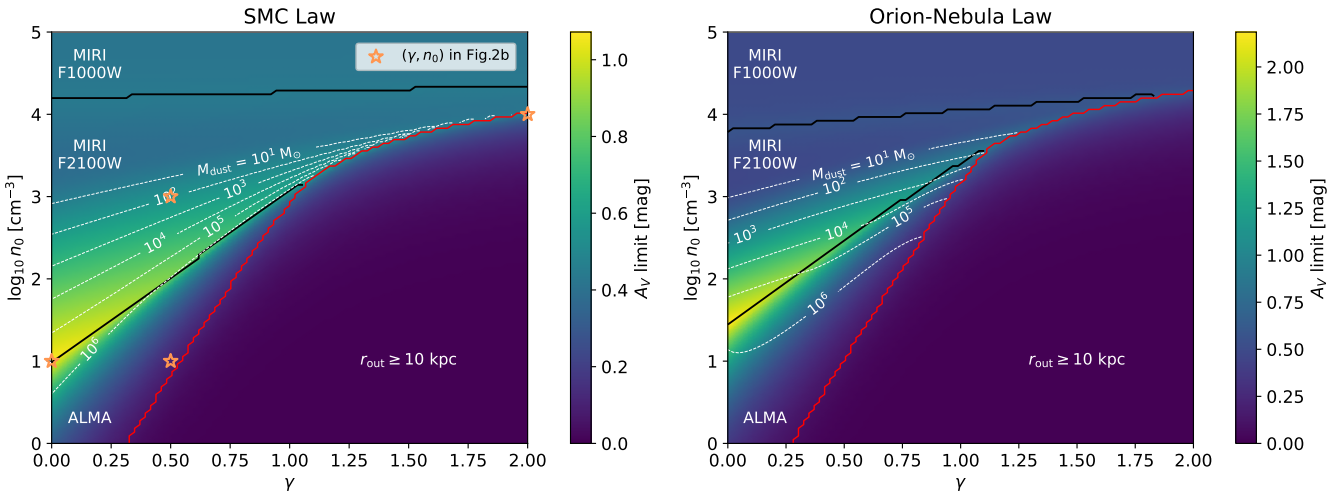

Figure 3. Parameter survey showing the upper limit on A_V as a function of the density distribution parameters (γ, n_0), assuming the SMC (left) and Orion Nebula (right) extinction curves. Black solid curves divide the regions where the maximum allowed A_V value is constrained by MIRI F1000W, F2100W, or ALMA data (from the top to the bottom). White dashed contours label the total dust mass $M_{\rm dust}$, computed using Equation (4) based on the corresponding A_V upper limit. Orange stars mark the density configurations shown in the right panel of Figure 2. The right-bottom region (i.e., steeper profiles with lower density normalization) requires extended dust distribution with $r_{\rm out} \geq 10$ kpc to achieve sufficient column density, and is therefore ruled out as unphysical configurations.

ence from the SMC case is that the Orion extinction law generally yields a higher A_V upper limit, reaching up to $\simeq 2$ mag around $(\gamma, n_0) \approx (0, 30\ {\rm cm}^{-3})$. This difference is primarily because the Orion extinction curve is significantly flatter in the UV range (see Figure 1). As a result, for a given A_V, the de-reddened intrinsic AGN spectrum is less luminous in the UV, leading to weaker reprocessed IR emission. Therefore, a higher A_V value is allowed without reprocessed IR fluxes exceeding the observed fluxes.

In both cases, the upper limit of A_V is obtained for a flat density profile ($\gamma \simeq 0$) with a normalization at $n_0 \simeq 10-30\ {\rm cm}^{-3}$. Given the dust distribution and corresponding A_V limit, the total dust mass is calculated by integrating the density profile from $r_{\rm in}$ to $r_{\rm out}$ (see Equation 4), as $M_{\rm dust} \sim 10^{5-6}\ M_\odot$. In the region below the boundary (black solid curve), the required dust mass increases and reaches up to $M_{\rm dust} < 10^7\ M_\odot$[4]. By contrast, the high-density regime allows for significantly lower dust mass. That is because the outer edge of the dusty medium becomes smaller in order to achieve the required column density for extinction, thereby reducing the total dust mass. In Section 4.1, we use the dust mass estimates to place additional constraints on the upper limit on A_V.

[4] The right-bottom region requires substantially extended dusty distributions with $r_{\rm out} \geq 10$ kpc. Such large radii yield infinitely large dust mass because $M_{\rm dust} \propto r_{\rm out}^{3-\gamma}$ for $\gamma < 3$.

We also note that previous studies have estimated dust masses for LRDs to be $M_{\rm dust} = 10^{3-5}\ M_\odot$ (C. M. Casey et al. 2024), assuming visual extinction $A_V \sim 3-4$ mag. These estimates are based on an effective size of $\langle R_{\rm e} \rangle \simeq 100$ pc measured in the F444W filter. The dust mass derived in our study is broadly consistent with these previous results, but tends to be higher by a factor of ~ 10. This is because our model determines the dust mass based on the physical extent of the dusty region, $r_{\rm out}$, which likely exceeds the effective size measured in the rest-frame optical, where dust does not emit. Recently, C. M. Casey et al. (2025) shows that the dust mass in LRDs is limited to $< 10^6\ M_\odot$ based on the non-detection of stacking deep ALMA observations for 60 LRDs, aligning well with our analysis.

3.3. *Model dependent A_V upper limits*

Figure 4 summarizes the upper limits on A_V derived for the two LRDs (A2744-45924 and RUBIES-BLAGN-1), using the three dust extinction laws based on observations and theoretical models (SMC, MW, and Orion) and a modified Calzetti law with $\delta = -1.8$ (see Equation 1). For each case, we show the least restrictive A_V upper limits across the entire (γ, n_0) parameter space (solid lines), under the condition that the total dust mass does not exceed a given threshold, $M_{\rm dust} \leq 10^4$, 10^5, or $10^6\ M_\odot$, as indicated by filled circles and bars. As expected, tighter constraints on $M_{\rm dust}$ result in a more stringent limit on the allowed A_V values.

For A2744-45924, the A_V upper limit increases from $\simeq 0.95^{+0.10}_{-0.13}$ mag for the SMC law to $\simeq 1.81^{+0.31}_{-0.37}$ mag for the Orion Nebula law. As described in Section 3.2, this trend originates from the differences in the UV slope of the extinction curve characterized by the ratio of $A_{\rm UV}/A_V$, where $A_{\rm UV}$ is the extinction level at 1215 Å. The SMC curve has a steep UV slope with $A_{\rm UV}/A_V \simeq 6.8$, while the MW and Orion curves are flatter ($\simeq 3.4$ and $\simeq 1.8$, respectively). Therefore, a steeper extinction curve in UV (i.e., higher $A_{\rm UV}/A_V$) results in stronger UV attenuation for a given A_V, leading to more reprocessed IR fluxes and thus to a stricter A_V upper limit. The extinction model with $\delta = -1.8$ of Equation (1) corresponds to a case with an extremely large slope of the extinction curve, $A_{\rm UV}/A_V \simeq 44$. Our analysis requires $A_V \leq 0.2$ mag; otherwise, the reprocessed IR emission exceeds the observational constraints.

For RUBIES-BLAGN-1, the A_V upper limits are generally higher than those for A2744-45924, ranging from $\simeq 1.34^{+0.11}_{-0.13}$ mag (SMC) to $\simeq 2.58^{+0.27}_{-0.36}$ mag (Orion). This results from the fact that RUBIES-BLAGN-1 exhibits weaker observed fluxes in rest-frame UV, which leads to a lower inferred intrinsic radiation flux for a given A_V. As a result, higher A_V values are permitted without exceeding the observed IR constraints.

We also remind readers that the least restrictive A_V is obtained for flat density profiles ($\gamma \simeq 0$) with $n_0 \simeq 10 - 30$ cm^{-3}. However, such profiles might be unphysical configurations, especially when considering the physical connection to the inner nucleus, see discussion in Section 4.3. Therefore, we also show the results for more concentrated density profiles with $\gamma \geq 1$ (dashed lines and open circles). These results are more stringent, yielding $\sim 50\%$ lower A_V upper limits.

As examined so far, the A_V upper limit depends on dust extinction laws, dust density distributions, dust mass requirements, and individual spectral features of LRDs. Nevertheless, the overall trend robustly suggests that the maximum allowed value $A_V^{\rm lim} \simeq 1$ mag in our analysis is significantly lower than the average value of $\langle A_V \rangle \simeq 3.48$ mag obtained from ~ 500 photometrically-selected LRD samples based on SED fitting analysis assuming obscured AGN scenarios (gray shaded region, H. B. Akins et al. 2024). In particular, with the SMC extinction law, the upper limit on A_V is reduced by $\Delta A_V \equiv \langle A_V \rangle - A_V^{\rm lim} \simeq 2.5$ mag. We will discuss the implications of this result to energetics for the entire LRD population in Section 4.2.

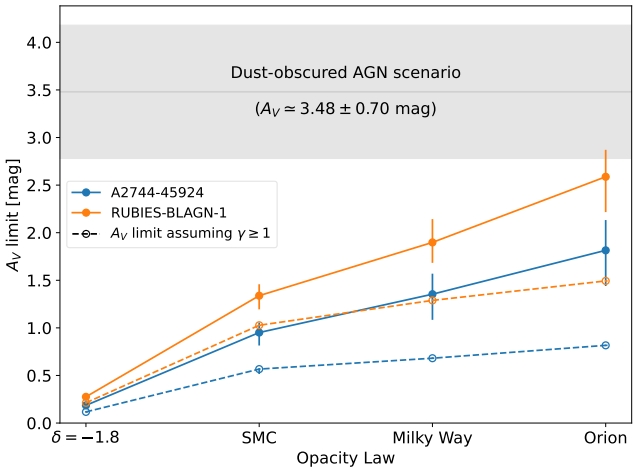

Figure 4. Summary of the upper limits on A_V derived for two representative LRDs: A2744-45924 and RUBIES-BLAGN-1. Each data point corresponds to the least restrictive A_V upper limit across the entire (γ, n_0) parameter space for dust masses $M_{\rm dust} \leq 10^4$, 10^5, and 10^6 $M_\odot$, shown as filled circles and bars for each extinction law: a modified Calzetti law with $\delta = -1.8$, SMC, MW, and Orion (from left to right). Dashed lines and open circles show the least restrictive A_V upper limits when imposing $\gamma \geq 1$. The gray shaded region indicates the extinction range typically assumed in obscured AGN scenarios ($A_V \simeq 3.48 \pm 0.70$ mag, H. B. Akins et al. 2024).

4. DISCUSSION

4.1. *Where were dust grains from?*

Our SED model provides not only the reprocessed IR spectrum but also an estimate of the dust mass for a given dust distribution. For the maximum allowed A_V, the corresponding dust mass is typically on the order of $M_{\rm dust} \lesssim 10^{5-6}$ $M_\odot$. Where do the amount of dust grains come from? In galaxies, dust grains are considered to form through stellar winds of evolved stars and from supernova ejecta, the latter of which is dominant in the early universe ($\lesssim 1$ Gyr). The dust production efficiency per unit stellar mass depends sensitively on the star formation history and the type of dust producers. Theoretical models estimate a dust-to-stellar mass ratio in the range of $f_{\rm dust,\star} \simeq 10^{-5} - 10^{-3}$, depending on whether supernova reverse shocks effectively destroy newly created dust grain in ejecta (see Figure 18 in R. Schneider & R. Maiolino 2024, and reference therein). Assuming a fiducial value of $f_{\rm dust,\star} = 10^{-4}$ for a constant star formation rate, the stellar mass required to produce $M_{\rm dust}$ is given by

$$M_\star \simeq 10^9 \; M_\odot \left(\frac{M_{\rm dust}}{10^5 \; M_\odot}\right) \left(\frac{f_{\rm dust,\star}}{10^{-4}}\right)^{-1}. \quad (7)$$

For A2744-45924, there is no clear host galaxy signature, but a faint, extended component is observed offset from the central LRD. Spectral and morphological analysis indicates that its unresolved host galaxy, if present, has a stellar mass of $M_\star < 10^{9.6}\ M_\odot$ within an effective radius of $R_e \simeq 70$ pc (I. Labbe et al. 2024; C.-H. Chen et al. 2025b). On the other hand, the extended component may be either a young low-mass galaxy ($M_\star \simeq 1.5 \times 10^8\ M_\odot$ and $t_{age} \simeq 15$ Myr, if assuming the same redshift as in the LRD; otherwise, it is a foreground galaxy at $z_{photo} \simeq 1.02$) or low-metallicity nebular emission ($Z \simeq 0.05\ Z_\odot$) powered by the LRD (C.-H. Chen et al. 2025a). These interpretations imply that the associated dust mass should be relatively low, $M_{dust} \lesssim (0.15\text{–}4) \times 10^5\ M_\odot$. For RUBIES-BLAGN-1, no host galaxy features are detected in imaging. However, spectral fitting using AGN+stellar composite models suggests $M_\star \simeq 1.8 \times 10^9\ M_\odot$, which is responsible for the observed rest-frame UV emission (B. Wang et al. 2024b). The stellar mass similarly implies a dust mass of $M_{dust} \lesssim 1.8 \times 10^5\ M_\odot$. In both cases, these dust mass estimates disfavor the least restrictive A_V upper limit obtained for a specific dust density profiles (see Figure 3), corresponding to $M_{dust} \sim 10^6\ M_\odot$. H. B. Akins et al. (2025) provided a dust mass upper limit for A2744-45924 and RUBIES-BLAGN-1 as $M_{dust} < 7 \times 10^7\ M_\odot$ and $< 1.4 \times 10^8\ M_\odot$ using the Rayleigh-Jeans tail of the SED in ALMA bands, respectively, and reported a tentative detection of the narrow [C I] line (809.34 GHz in rest-frame) with FWHM $\simeq 80$ km s^{-1} in A2744-45924, implying a dynamical mass of $\lesssim 10^{10}\ M_\odot$. These mass estimates are consistent with our analysis. Future improvements of stellar mass measurements provide more stringent limits on the dust content and extinction in LRDs, making the dust budget crisis severer.

While our argument does not provide a lower limit on A_V since we make no assumption about the intrinsic SED and instead reconstruct it through spectral dereddening, some SED models for LRDs with a prominent Balmer break require extremely high hydrogen column densities $N_H \gtrsim 10^{25}$ cm^{-2} but adopt only modest extinction levels of $A_V \sim 0.2 - 0.5$ mag (R. P. Naidu et al. 2025; A. J. Taylor et al. 2025). These models implicitly assume that the dust-to-gas mass ratio in such LRDs is $\lesssim 10^{-4}$ of the canonical solar-neighborhood value $\mathcal{D}_\odot = 0.01$. This suggests that at least some LRDs might emerge from extremely low-metallicity (or pristine) environments with $Z \sim 10^{-4}\ Z_\odot$ or under peculiar conditions where dust grains formation is strongly suppressed. Recently, several theoretical studies have proposed spectral models that yield *intrinsically red* optical continua without relying on dust reddening: dense gaseous envelopes surrounding BHs (D. Kido et al. 2025), circum-binary disks around coalescing BHs (K. Inayoshi et al. 2025), and self-gravitating disks (C. Zhang et al. 2025).

4.2. *Sołtan–Paczyński argument*

Compiling data from extensive AGN surveys, we constrain the radiative efficiency of BHs by comparing the observed BH mass density ρ_{BH} to the mass accretion rate to BHs inferred from the luminosity density $\mathcal{L}$ per comoving volume in earlier epochs, known as the Sołtan–Paczyński argument (A. Soltan 1982; Q. Yu & S. Tremaine 2002). This analysis suggests a radiative efficiency $\epsilon_{rad} \simeq 10\%$ for AGNs at $0 < z < 5$ and favors modest spins of these BHs under geometrically-thin disk configuration (I. D. Novikov & K. S. Thorne 1973; N. I. Shakura & R. A. Sunyaev 1973). The same argument has been applied to LRD populations (K. Inayoshi & K. Ichikawa 2024) by quantifying ρ_{BH} and $\mathcal{L}$ through integrating the LRD luminosity function and BH mass functions, respectively, under the assumption of obscured AGNs (J. Matthee et al. 2024; V. Kokorev et al. 2024; H. B. Akins et al. 2024; J. E. Greene et al. 2024). The radiative efficiency results in $\epsilon_{rad} \simeq 20\%$, suggesting rapid BH spins with 96% of the maximum limit.

We here revisit the Sołtan-Paczyński argument for LRD populations by accounting for our conclusion that the LRD spectral features do not necessarily require heavy dust reddening of AGNs. Instead, the level of extinction must be modest ($A_V \lesssim 1$ mag) to remain consistent with MIRI detection and ALMA non-detection. This revised extinction enables a re-evaluation of both the intrinsic AGN luminosity and single-epoch virial BH mass, $M_{BH} \propto L^{1/2}$ (e.g., S. Kaspi et al. 2005), using the broad-line region luminosity-size empirical relation calibrated via reverberation mapping for nearby AGNs. Here, L refers to the AGN continuum luminosity at rest-frame 5100 Å or the luminosity of the broad Hα (Hβ) emission line (e.g., J. E. Greene & L. C. Ho 2005; A. E. Reines et al. 2013), both of which are dust corrected using the inferred visual extinction A_V as they lie at similar wavelengths. Therefore, the impact on the inferred radiative efficiency ϵ_{rad} can be quantified as

$$\frac{\epsilon_{rad}}{1-\epsilon_{rad}} = \frac{\int_0^{t_0} \mathcal{L}(t)dt}{\rho_{BH}(t_0)c^2} \simeq 0.25 \cdot 10^{-0.2\Delta A_V},$$
$$\rightarrow 0.079 \quad \text{with } \Delta A_V = 2.5 \text{ mag}, \qquad (8)$$

where t_0 is the cosmic time at $z = 4$ when the BH mass density is measured, $\Delta A_V = \langle A_V \rangle - A_V^{lim}$ (see Section 3.3), and the prefactor of 0.25 is the best-fitted value

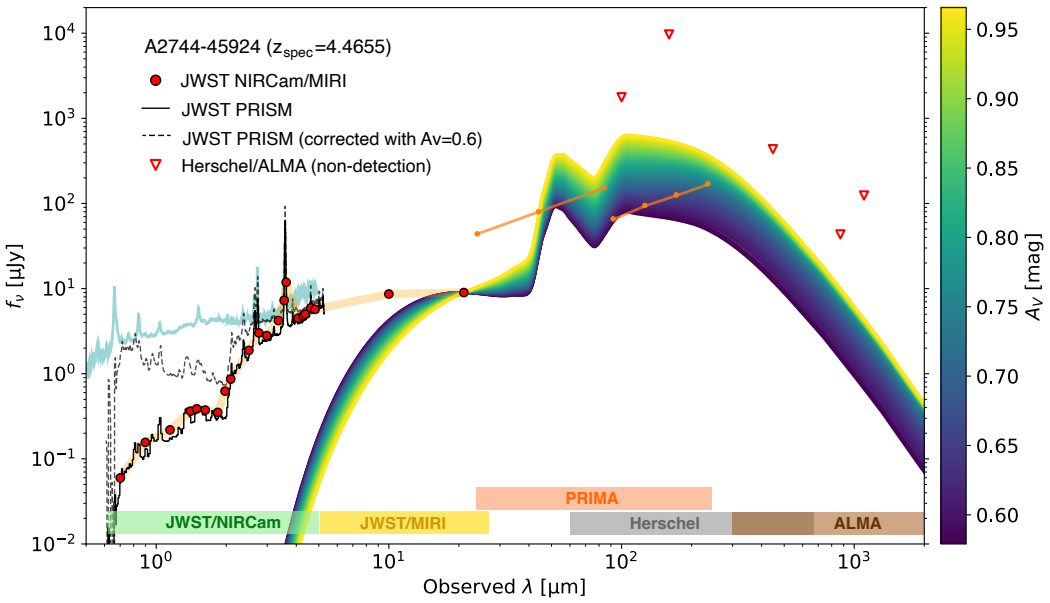

Figure 5. Observed flux densities (f_ν) of the brightest LRD (A2744-45924) at $z_{\rm spec} = 4.4655$, comparing modeled dust re-emission with current observational data and future detection capabilities with PRIMA. Observed photometric data points for A2744-45924 are shown in circles and triangles, together with the JWST spectrum (black line). The colored curves represent the maximum predicted IR re-emission flux densities from various dust distribution models, each calculated to be consistent with existing observational constraints from JWST MIRI and ALMA, with the colors indicating the derived upper limit on visual extinction (A_V) for each model. All models presented correspond to a fixed dust mass of $M_{\rm dust} = 10^5\ M_\odot$. The black dashed curve presents the expected intrinsic spectrum with dust correction assuming $A_V = 0.6$ mag, which does not agree with the shape of the low-z AGN composite spectral template (cyan, D. E. Vanden Berk et al. 2001). The orange lines indicate the anticipated 5σ sensitivity for a 20-hour PRIMA exposure for 10 arcmin^2 areas. Colored boxes at the bottom illustrate the wavelength coverage of relevant telescopes and instruments.

($\epsilon_{\rm rad} \simeq 20\%$; K. Inayoshi & K. Ichikawa 2024) under the assumption of obscured AGNs with $\langle A_V \rangle \simeq 3.48$ mag (H. B. Akins et al. 2024). With the revised A_V constraint in this work, we find a radiative efficiency of $\epsilon_{\rm rad} \simeq 0.073$, which aligns well with the canonical 10% radiative efficiency (Q. Yu & S. Tremaine 2002; Y. Ueda et al. 2014; I. Delvecchio et al. 2014)[5]. Thus, this resolves the apparent tension with the classical Sołtan argument for the LRD population (K. Inayoshi & K. Ichikawa 2024).

4.3. *Physical connection to the inner nucleus*

We examine how the A_V upper limit depends on the dust density distribution, using the observed spectral of A2744-45924 and RUBIES-BLAGN-1, both of which show a Balmer break feature (B. Wang et al. 2024b; I. Labbe et al. 2024). A recently proposed interpretation attributes this spectral break to absorption by dense gas with $n_{\rm cl} \gtrsim 10^9$ cm^{-3}, where atomic hydrogen is excited to the $n = 2$ states via particle collision (K. Inayoshi & R. Maiolino 2025; X. Ji et al. 2025). These absorbers can imprint the Balmer-break feature on their spectra as well as Balmer absorption on Hβ and Hα emission. This scenario motivates us to explore the possible physical connection between the dense gas clouds in or just outside the broad-line region (BLR; $r_{\rm BLR} \sim 0.01$ pc) and the dusty media near the sublimation radius ($r_{\rm sub} \sim 1$ pc). Assuming that the gas density follows a power-law radial profile with the same index γ as in the dusty region, the density at $r = r_{\rm sub}$ is given by

$$n_0 \simeq \frac{n_{\rm cl}}{\mathcal{C}} \left(\frac{r_{\rm BLR}}{r_{\rm sub}} \right)^{\gamma}, \tag{9}$$

where $\mathcal{C}$ is the density enhanced factor caused by cloud clumpiness and shock-compression in outflowing materials. Here, we set $\mathcal{C} = 10$, though the true value may be smaller given the high covering fraction required by the absorption features (R. Maiolino et al. 2025; K. Inayoshi & R. Maiolino 2025).

[5] This low value of $\epsilon_{\rm rad} \simeq 0.073$ is consistent with that of non-spinning BHs under the thin-disk approximation, or possibly indicates a low radiative efficiency due to photon trapping in super-Eddington slim disks around BHs with moderate spins of $a_{\rm BH} \simeq 0.7$ (M. A. Abramowicz et al. 1988; K. Ohsuga et al. 2005; K. Inayoshi et al. 2020)

With this scaling, a profile slope of $\gamma = 2$ suggests $n_0 \simeq 10^4$ cm^{-3}, while shallower slopes ($\gamma < 2$) yield even higher n_0 values. As shown in Figure 3, the least constrained A_V upper limits arise from a flat density profile ($\gamma \simeq 0$) with $n_0 \simeq 10$–30 cm^{-3}. However, if the density profile indeed connects the BLR and dust sublimation scales as suggested above, such flat profiles are disfavored. In particular, for $\gamma = 2$ and $n_0 = 10^4$ cm^{-3}, the extinction level required to satisfy the MIRI and ALMA constraints is significantly lower, with $A_V^{\rm lim} \simeq 0.41$ mag.

4.4. *Direct test with PRIMA*

Figure 5 presents the compiled SED models for A2744-45924 at $z_{\rm spec} = 4.4655$ that are consistent with the observational constraints from the JWST MIRI and ALMA. The color code indicates the upper limits on A_V for a fixed dust mass of $M_{\rm dust} = 10^5\ M_\odot$, assuming the SMC extinction curve. For illustration, the expected intrinsic spectrum with dust correction assuming $A_V = 0.6$ mag is shown (black dashed), which does not match the low-z AGN spectrum template (cyan, D. E. Vanden Berk et al. 2001).

Despite the deep MIRI and ALMA observations, the rest-frame MIR spectral shape remains largely unconstrained due to the relatively shallow limits from Herschel data. The PRobe for-Infrared Mission for Astrophysics (PRIMA) is expected to significantly improve MIR sensitivity for extragalactic astronomy[6]. We overlay the expected 5σ sensitivity of a 20-hour survey over 10 arcmin^2 using the PRIMAger mode, which offers hyperspectral narrow-band imaging ($R = 10$) from 24 to 84 μm and four polarimetry broad band channels between 96 and 235 μm (see more details in A. Moullet et al. 2023)[7]. The PRIMA detection limit of ~ 100 μJy is more than two orders of magnitude deeper than that of Herschel/PACS under a similar survey design. This PRIMA capability enables MIR detection for most of the SED cases presented, bringing opportunities to investigate key diagnostic features such as the 9.7 μm silicate emission/absorption and PAH emission (although our current SEDs do not have PAH features).

If the MIR fluxes remain undetected by the PRIMA survey with the expected detection threshold, the upper limit on A_V will be further tightly constrained to $A_V \lesssim 0.62$ mag. The future PRIMAger survey program is an ideal platform to test our model and related theoretical interpretations for the LRD properties.

Furthermore, the modeling framework presented herein is both robust and readily applicable, offering a powerful tool to derive crucial upper limits on dust extinction and dust mass for any LRD with UV-to-IR photometric or spectroscopic data available. Such constraints are vital for unveiling the true nature of LRDs and will be valuable for maximizing the scientific yield from ongoing and upcoming surveys.

ACKNOWLEDGMENTS

We greatly thank Hollis B. Akins, Changhao Chen, Kohei Ichikawa, Yue Liu, Masafusa Onoue, and Jinyi Shangguan for constructive discussions. K. I. and L. C. H. acknowledge support from the National Natural Science Foundation of China (12233001), the National Key R&D Program of China (2022YFF0503401), and the China Manned Space Program (CMS-CSST-2025-A09). The modeling code developed in this work is publicly available at https://github.com/c-kj/LRD_dust_modeling.

AUTHOR CONTRIBUTIONS

The first two authors (K. Chen and Z. Li) equally contributed to this work.

Software: Astropy (Astropy Collaboration et al. 2022), dust_extinction(K. D. Gordon 2024), Cloudy (C. M. Gunasekera et al. 2023)

REFERENCES

Abramowicz, M. A., Czerny, B., Lasota, J. P., & Szuszkiewicz, E. 1988, ApJ, 332, 646, doi: 10.1086/166683

Akins, H. B., Casey, C. M., Lambrides, E., et al. 2024, arXiv e-prints, arXiv:2406.10341, doi: 10.48550/arXiv.2406.10341

Akins, H. B., Casey, C. M., Chisholm, J., et al. 2025, arXiv e-prints, arXiv:2503.00998, doi: 10.48550/arXiv.2503.00998

Astropy Collaboration, Price-Whelan, A. M., Lim, P. L., et al. 2022, ApJ, 935, 167, doi: 10.3847/1538-4357/ac7c74

Baldwin, J. A., Ferland, G. J., Martin, P. G., et al. 1991, ApJ, 374, 580, doi: 10.1086/170146

Barro, G., Pérez-González, P. G., Kocevski, D. D., et al. 2024, ApJ, 963, 128, doi: 10.3847/1538-4357/ad167e

Barvainis, R. 1987, ApJ, 320, 537, doi: 10.1086/165571

[6] https://prima.ipac.caltech.edu/

[7] https://prima.ipac.caltech.edu/page/etc-calc

Baskin, A., & Laor, A. 2018, MNRAS, 474, 1970, doi: 10.1093/mnras/stx2850

Calzetti, D., Armus, L., Bohlin, R. C., et al. 2000, ApJ, 533, 682, doi: 10.1086/308692

Casey, C. M., Akins, H. B., Kokorev, V., et al. 2024, ApJL, 975, L4, doi: 10.3847/2041-8213/ad7ba7

Casey, C. M., Akins, H. B., Finkelstein, S. L., et al. 2025, arXiv e-prints, arXiv:2505.18873. https://arxiv.org/abs/2505.18873

Chen, C.-H., Ho, L. C., Li, R., & Inayoshi, K. 2025a, arXiv e-prints, arXiv:2505.03183, doi: 10.48550/arXiv.2505.03183

Chen, C.-H., Ho, L. C., Li, R., & Zhuang, M.-Y. 2025b, ApJ, 983, 60, doi: 10.3847/1538-4357/ada93a

de Graaff, A., Rix, H.-W., Naidu, R. P., et al. 2025, arXiv e-prints, arXiv:2503.16600, doi: 10.48550/arXiv.2503.16600

Delvecchio, I., Gruppioni, C., Pozzi, F., et al. 2014, MNRAS, 439, 2736, doi: 10.1093/mnras/stu130

Draine, B. T. 2011, Physics of the Interstellar and Intergalactic Medium

Euclid Collaboration, Bisigello, L., Rodighiero, G., et al. 2025, arXiv e-prints, arXiv:2503.15323, doi: 10.48550/arXiv.2503.15323

Fujimoto, S., Brammer, G. B., Watson, D., et al. 2022, Nature, 604, 261, doi: 10.1038/s41586-022-04454-1

Gordon, K. D. 2024, Journal of Open Source Software, 9, 7023, doi: 10.21105/joss.07023

Greene, J. E., & Ho, L. C. 2005, ApJ, 630, 122, doi: 10.1086/431897

Greene, J. E., Labbe, I., Goulding, A. D., et al. 2024, ApJ, 964, 39, doi: 10.3847/1538-4357/ad1e5f

Gunasekera, C. M., van Hoof, P. A. M., Chatzikos, M., & Ferland, G. J. 2023, Research Notes of the American Astronomical Society, 7, 246, doi: 10.3847/2515-5172/ad0e75

Hainline, K. N., Maiolino, R., Juodžbalis, I., et al. 2025, ApJ, 979, 138, doi: 10.3847/1538-4357/ad9920

Hao, L., Weedman, D. W., Spoon, H. W. W., et al. 2007, ApJL, 655, L77, doi: 10.1086/511973

Hönig, S. F., & Kishimoto, M. 2010, A&A, 523, A27, doi: 10.1051/0004-6361/200912676

Inayoshi, K. 2025, arXiv e-prints, arXiv:2503.05537, doi: 10.48550/arXiv.2503.05537

Inayoshi, K., & Ichikawa, K. 2024, arXiv e-prints, arXiv:2402.14706, doi: 10.48550/arXiv.2402.14706

Inayoshi, K., & Maiolino, R. 2025, ApJL, 980, L27, doi: 10.3847/2041-8213/adaebd

Inayoshi, K., Shangguan, J., Chen, X., Ho, L. C., & Haiman, Z. 2025, arXiv e-prints, arXiv:2505.05322, doi: 10.48550/arXiv.2505.05322

Inayoshi, K., Visbal, E., & Haiman, Z. 2020, ARA&A, 58, 27, doi: 10.1146/annurev-astro-120419-014455

Ji, X., Maiolino, R., Übler, H., et al. 2025, arXiv e-prints, arXiv:2501.13082, doi: 10.48550/arXiv.2501.13082

Kaspi, S., Maoz, D., Netzer, H., et al. 2005, ApJ, 629, 61, doi: 10.1086/431275

Kido, D., Ioka, K., Hotokezaka, K., Inayoshi, K., & Irwin, C. M. 2025, arXiv e-prints, arXiv:2505.06965, doi: 10.48550/arXiv.2505.06965

Killi, M., Watson, D., Brammer, G., et al. 2024, A&A, 691, A52, doi: 10.1051/0004-6361/202348857

Kocevski, D. D., Onoue, M., Inayoshi, K., et al. 2023, ApJL, 954, L4, doi: 10.3847/2041-8213/ace5a0

Kocevski, D. D., Finkelstein, S. L., Barro, G., et al. 2024, arXiv e-prints, arXiv:2404.03576, doi: 10.48550/arXiv.2404.03576

Kokorev, V., Fujimoto, S., Labbe, I., et al. 2023, ApJL, 957, L7, doi: 10.3847/2041-8213/ad037a

Kokorev, V., Caputi, K. I., Greene, J. E., et al. 2024, ApJ, 968, 38, doi: 10.3847/1538-4357/ad4265

Labbe, I., Greene, J. E., Matthee, J., et al. 2024, arXiv e-prints, arXiv:2412.04557, doi: 10.48550/arXiv.2412.04557

Labbe, I., Greene, J. E., Bezanson, R., et al. 2025a, ApJ, 978, 92, doi: 10.3847/1538-4357/ad3551

Labbe, I., Greene, J. E., Bezanson, R., et al. 2025b, ApJ, 978, 92, doi: 10.3847/1538-4357/ad3551

Leung, G. C. K., Finkelstein, S. L., Pérez-González, P. G., et al. 2024, arXiv e-prints, arXiv:2411.12005, doi: 10.48550/arXiv.2411.12005

Li, Z., Inayoshi, K., Chen, K., Ichikawa, K., & Ho, L. C. 2025, ApJ, 980, 36, doi: 10.3847/1538-4357/ada5fb

Ma, Y., Greene, J. E., Setton, D. J., et al. 2025a, arXiv e-prints, arXiv:2504.08032, doi: 10.48550/arXiv.2504.08032

Ma, Y., Greene, J. E., Setton, D. J., et al. 2025b, ApJ, 981, 191, doi: 10.3847/1538-4357/ada613

Maiolino, R., Risaliti, G., Signorini, M., et al. 2025, MNRAS, 538, 1921, doi: 10.1093/mnras/staf359

Matthee, J., Naidu, R. P., Brammer, G., et al. 2024, ApJ, 963, 129, doi: 10.3847/1538-4357/ad2345

Moullet, A., Kataria, T., Lis, D., et al. 2023, arXiv e-prints, arXiv:2310.20572, doi: 10.48550/arXiv.2310.20572

Naidu, R. P., Matthee, J., Katz, H., et al. 2025, arXiv e-prints, arXiv:2503.16596. https://arxiv.org/abs/2503.16596

Nenkova, M., Sirocky, M. M., Ivezić, Ž., & Elitzur, M. 2008, ApJ, 685, 147, doi: 10.1086/590482

Noll, S., Burgarella, D., Giovannoli, E., et al. 2009, A&A, 507, 1793, doi: 10.1051/0004-6361/200912497

Novikov, I. D., & Thorne, K. S. 1973, in Black Holes (Les Astres Occlus), 343–450

Ohsuga, K., Mori, M., Nakamoto, T., & Mineshige, S. 2005, ApJ, 628, 368, doi: 10.1086/430728

Pérez-González, P. G., Barro, G., Rieke, G. H., et al. 2024, ApJ, 968, 4, doi: 10.3847/1538-4357/ad38bb

Reach, W. T., Boulanger, F., Contursi, A., & Lequeux, J. 2000, A&A, 361, 895, doi: 10.48550/arXiv.astro-ph/0007382

Reines, A. E., Greene, J. E., & Geha, M. 2013, ApJ, 775, 116, doi: 10.1088/0004-637X/775/2/116

Rinaldi, P., Bonaventura, N., Rieke, G. H., et al. 2024, arXiv e-prints, arXiv:2411.14383, doi: 10.48550/arXiv.2411.14383

Schneider, R., & Maiolino, R. 2024, A&A Rv, 32, 2, doi: 10.1007/s00159-024-00151-2

Setton, D. J., Greene, J. E., de Graaff, A., et al. 2024, arXiv e-prints, arXiv:2411.03424, doi: 10.48550/arXiv.2411.03424

Setton, D. J., Greene, J. E., Spilker, J. S., et al. 2025, arXiv e-prints, arXiv:2503.02059, doi: 10.48550/arXiv.2503.02059

Shakura, N. I., & Sunyaev, R. A. 1973, A&A, 24, 337

Soltan, A. 1982, MNRAS, 200, 115

Taylor, A. J., Kokorev, V., Kocevski, D. D., et al. 2025, arXiv e-prints, arXiv:2505.04609, doi: 10.48550/arXiv.2505.04609

Ueda, Y., Akiyama, M., Hasinger, G., Miyaji, T., & Watson, M. G. 2014, ApJ, 786, 104, doi: 10.1088/0004-637X/786/2/104

Vanden Berk, D. E., Richards, G. T., Bauer, A., et al. 2001, AJ, 122, 549, doi: 10.1086/321167

Wang, B., Leja, J., de Graaff, A., et al. 2024a, ApJL, 969, L13, doi: 10.3847/2041-8213/ad55f7

Wang, B., de Graaff, A., Davies, R. L., et al. 2024b, arXiv e-prints, arXiv:2403.02304, doi: 10.48550/arXiv.2403.02304

Weingartner, J. C., & Draine, B. T. 2001, ApJ, 548, 296, doi: 10.1086/318651

Xiao, M., Oesch, P. A., Bing, L., et al. 2025, arXiv e-prints, arXiv:2503.01945, doi: 10.48550/arXiv.2503.01945

Yu, Q., & Tremaine, S. 2002, MNRAS, 335, 965, doi: 10.1046/j.1365-8711.2002.05532.x

Zhang, C., Wu, Q., Fan, X., et al. 2025, arXiv e-prints, arXiv:2505.12719, doi: 10.48550/arXiv.2505.12719